A Geometric Matched Filter for Hyperspectral Target Detection and Partial Unmixing

Muhammad Awais Akhter, Rob Heylen, and Paul Scheunders

***Abstract*—In this letter, a new geometric matched filter (MF) is proposed by combining the standard MF with concepts of convex geometry. The purpose of the method is twofold: for subpixel target detection and for partial unmixing of a hyperspectral image. In standard matched filtering, the filter is designed based on the background statistics of the entire image, which works fine for rare targets but fails when the target is frequently present throughout the whole image. In the presented method, the background is restricted to pixels that have a zero contribution to the target spectrum. These background pixels are identified based on the simplex formed by the target and other relevant endmembers of the data set. Experiments are conducted for the specific case of targets which are frequently present in an image. The presented method is shown to outperform standard matched filtering and orthogonal subspace projection for target detection, and for the estimation of the target abundances.**

***Index Terms*—Hyperspectral, matched filter (MF), partial unmixing, target detection.**

I. Introduction

HYPERSPECTRAL imagery characterizes ground cover materials based on their spectral reflectance. The limited spatial resolution of hyperspectral images, however, causes pixels to contain mixtures of different materials. In mixed pixels, the spectrum is a combination of the constituent materials (endmembers) present in the scene [1]. Spectral unmixing techniques decompose the pixel spectrum into its constituent materials and calculate the fractional presence (abundances) of each material. In the linear mixing model, the spectra of mixed pixels are assumed to be a linear combination of endmembers, and the weights represent the relative abundances of each material within the pixel.

A complete spectral unmixing of hyperspectral data may not always be possible or required. In subpixel target detection, the aim is to detect whether a particular target spectrum is present within the pixel spectrum, without having to know the target's specific relative contribution [2]. Sometimes, a partial unmixing, i.e., the determination of the relative contribution of one or a few target spectra, is aimed for [3].

To date, various algorithms have been developed for unmixing-based target detection and partial unmixing. In particular, subspace-based target detection methods project the data onto the subspace orthogonal to the background. The background subspace can be estimated in a structured manner, in which the background is modeled using endmembers. In [4], an orthogonal subspace projection (OSP) method was proposed for this purpose. In [5], it was shown that OSP is identical to full (unconstrained) unmixing. On the other hand, in a stochastic approach, no background modeling is applied. In [3], a matched filter (MF) detector was proposed in which the background is estimated from the eigenvectors of the data correlation matrix or from the singular vector of the data matrix. This was further elaborated in [6]. In [7], k-means clustering was used to improve the MF detection process. Recently, in [8], a feasibility measure has been added to reduce false alarms. In [9], an analytical comparison between the model-based and the statistical approach was performed. In [10], a hybrid target detector was proposed that combines the statistical and model-based approaches. Sometimes, the target abundance values are to be estimated as well. In [11], an overview of subspace-based partial unmixing methods is given. In [12], it was shown that, under certain conditions, the whitened version of matched filtering, constrained energy minimization, delivers fractional abundances.

A problem with the background-based detection methods is that target-signal components may be included in the background estimation, causing target leakage. One of the causes of this problem is an overestimation of the dimensionality of the background subspace. The effect of the dimensionality is studied in [13] and [14] for the MF and in [15] for OSP. In [16], sparse representations were applied to reduce the dimensionality effects. A local estimation of the background was proposed in [17].

Other recent topics that were treated in the literature are the problem of false alarm mitigation [18], target variability [19], nonlinear kernel-based target detection [20], and sparsity in target detection [21]. For a recent signal-processing-oriented overview of the state of the art on hyperspectral target detection, see [2] and [22].

Background subspace methods are likely to only work when "rare" targets are aimed for, i.e., having a contribution to only a very small subset of the pixels. When a target is more frequently present in the data cube, the background statistics is wrongly influenced by the target contribution, again causing target leakage. In this letter, we regard the problem of "frequent target" detection in data with many pixels containing the target, albeit with low abundances, as may be the case in, e.g., mineral detection. To mitigate the dependence on the particular number and choice of endmembers in the model-based approaches and the target influence on the background statistics in the stochastic approaches, we present a new hybrid target detection method

Manuscript received April 24, 2014; revised July 17, 2014 and August 18, 2014; accepted September 4, 2014. Date of publication September 25, 2014; date of current version October 8, 2014. This work was supported in part by the Flemish Agency for Innovation by Science and Technology (IWT) through the project CHAMELEON. The work of R. Heylen was supported by the Research Foundation Flanders (FWO).

The authors are with the iMinds-Visionlab, University of Antwerp, 2610 Antwerp, Belgium (e-mail: muhammadawais.akhter@uantwerpen.be; rob.heylen@uantwerpen.be; paul.scheunders@uantwerpen.be).

Color versions of one or more of the figures in this paper are available online at http://ieeexplore.ieee.org.

Digital Object Identifier 10.1109/LGRS.2014.2355915

combining spectral unmixing and matched filtering, making use of convex geometry concepts.

First, we model the background by a number of endmembers, obtained, e.g., from an unsupervised endmember extraction method. Then, using the geometry of the simplex spanned by these endmembers, a number of pixels that have zero abundance values for the target are determined and used for the background estimation in an MF. In the experimental section, we show that, indeed, the proposed method is robust against the specific choice and number of endmembers as compared to OSP. It is shown that, as opposed to MF, the method performs well for rare targets as well as for nonrare targets. Moreover, the method obtains more accurate target fractions. In the next section, the methodology is explained, followed by the experiments and discussion in Section III.

II. Methodology

Consider a hyperspectral image with d spectral bands and a known target spectrum $\mathbf{t_s}$. The aim of the proposed method is to identify the target signature in the presence of a mixed background, where we assume that the target is frequently present. A pixel spectrum can then be modeled as

$$\mathbf{x} = \gamma \cdot \mathbf{t_s} + \mathbf{b} \tag{1}$$

where γ is the target abundance value and $\mathbf{b}$ represents the background. Usually, target detection is defined by as a binary hypothesis testing problem for testing the null hypothesis H_0 : $\gamma = 0$ versus the alternative hypothesis $H_1 : \gamma > 0$.

Methods to solve this problem differ in the way that the background is modeled.

A. OSP

In OSP, it is assumed that the background can be explained by a linear mixture model (LMM), so that the model becomes

$$\mathbf{x} = \gamma \cdot \mathbf{t_s} + \sum_{i=1}^{p} a_i \mathbf{e_i} + \epsilon \tag{2}$$

where $\mathbf{e_i}$ denotes the p endmembers $\{\mathbf{e}_1, \mathbf{e}_2, \ldots, \mathbf{e_p}\}$ $(p < d)$, the coefficients a_i represents the abundances for each endmember, and ϵ is the additive noise.

In OSP, the spectra are projected onto the subspace orthogonal to the background, using the projection operator $P^{\perp} = \mathbf{I} - \hat{\mathbf{E}}(\hat{\mathbf{E}}^{\mathrm{T}}\hat{\mathbf{E}})^{-1}\hat{\mathbf{E}}^{\mathrm{T}}$, where $\hat{\mathbf{E}}$ is the matrix of endmembers excluding the target. The OSP detector is then given as the least squares estimator of γ in model (2)

$$\mathrm{OSP}(\mathbf{x}) = \frac{\mathbf{x^T} P^{\perp} \mathbf{t_s}}{\mathbf{t_s^T} P^{\perp} \mathbf{t_s}} \gtrless_{H_0}^{H_1} \tau_{\mathrm{OSP}} \tag{3}$$

where τ_{OSP} is a threshold. The detector performance is commonly measured by means of a receiver operating characteristic (ROC) curve, by varying the threshold value and comparing the true positive against the false positive detection rate. The denominator in (3) normalizes the result for a perfect target match to one. A clear disadvantage of this method is that it relies severely on the number and the specific choice of endmembers [15].

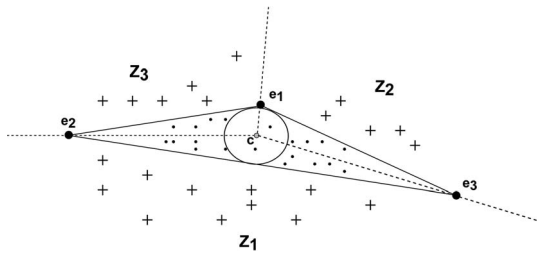

Fig. 1. Two-dimensional simplex with three endmembers $(\mathbf{e_1}, \mathbf{e_2}, \mathbf{e_3})$, incenter $\mathbf{c}$, and bisective cones (Z_1, Z_2, Z_3); ·'s and +'s indicate points inside and outside the simplex, respectively. Points in the cone Z_i but outside the simplex have zero contribution from $\mathbf{e_i}$.

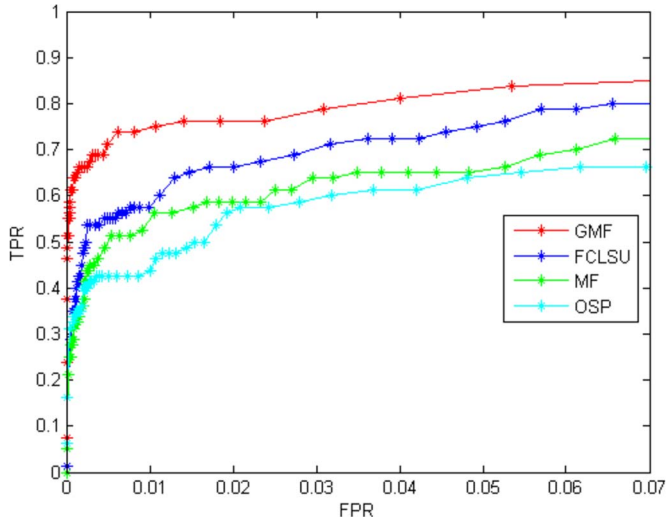

Fig. 2. ROC curve for FCLSU, OSP, MF, and GMF.

B. MF

In the case where the background is not modeled by endmembers, but statistically estimated from the data, an MF is obtained.

The MF detector is obtained as the least squares estimator of γ in model (1) [11]

$$\mathrm{MF}(\mathbf{x}) = \frac{\mathbf{x}^{\mathrm{T}} \mathbf{C^{-1}} \mathbf{t_s}}{\mathbf{t_s^T} \mathbf{C^{-1}} \mathbf{t_s}} \gtrless_{H_0}^{H_1} \tau_{\mathrm{MF}} \tag{4}$$

where $\mathbf{C^{-1}}$ is the inverse of the covariance matrix estimated from the background. The denominator in (4) normalizes the result for a perfect target match to one. In practice, the mean spectrum is first subtracted from the data, making the data zero mean. For "rare" targets, the background covariance can be reliably estimated from all pixels of the data cube. If the targeted material is frequently present in the image, the background will be wrongly influenced by pixels containing the target.

C. GMF

In the following, we will describe a hybrid method combining the model-based OSP and statistics-based MF approaches. The LMM will be used for the identification of pixels that do not contain the target. These identified pixels will then be used to estimate the background covariance matrix in an improved MF.

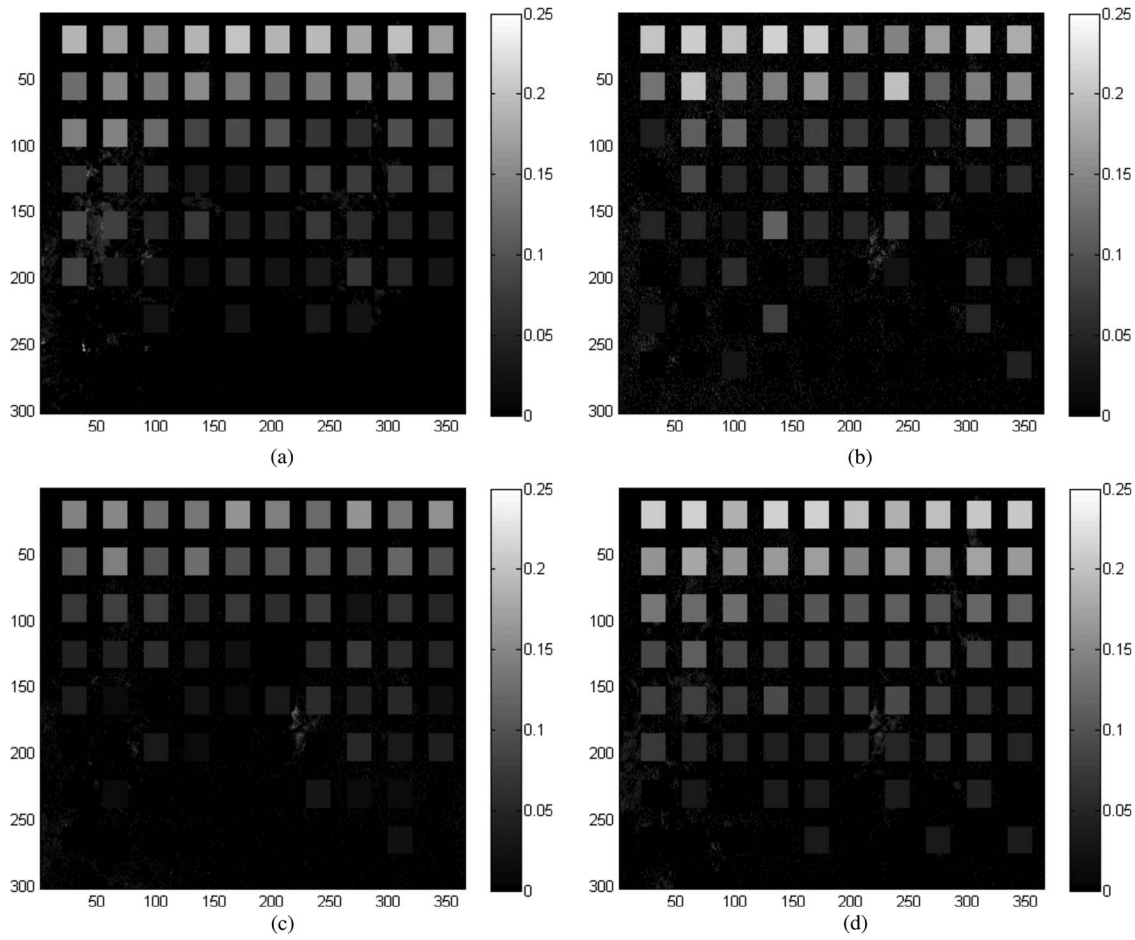

Fig. 3. (a)–(d) Detector output for a fixed FPR of 0.07 using FCLSU, OSP, MF, and GMF, respectively.

To present the method, we will rely on the geometric interpretation of the LMM. In geometric terms, the p endmembers form a simplex in a $(p-1)$-dimensional affine subspace of the d-dimensional data space. The first step is actually to project the data on the simplex plane, formed by the endmembers, including the target endmember (this is the plane formed by the affine span of the endmembers, i.e., all linear combinations given that the coefficients sum up to one). This automatically takes care of the abundance sum-to-one constraint. It is important to notice that, for high-dimensional data (as hyperspectral data are), after this projection, many data points will fall outside the actual simplex, which means that these pixels do not obey the abundance positivity constraint. In fact, this is a consequence of the curse of dimensionality. For a reasonable amount of endmembers, the volume of the simplex will be that small that it is highly improbable that a point falls inside it.

The background pixels are estimated based on this observation and the following two observations [23].

1) A point lying in the simplex plane, but outside the simplex, has at least one zero abundance coefficient.
2) To estimate the zero abundance coefficient, the bisective cones (i.e., the planes that bisect the dihedral angles between the faces of the simplex) can be used.

First, the incenter $\mathbf{c}$ of a simplex S is defined as the intersection of all $(p-2)$-dimensional planes that bisect the dihedral angles between the faces of the simplex. It is also the center of the largest possible hypersphere inscribed in the simplex. Let

TABLE I
OBTAINED AVERAGE (STANDARD DEVIATION) ABUNDANCE VALUES FOR EACH TARGET ROW OF Fig. 3

True	GMF	FCLSU	OSP	MF
.20	**0.202** (0.010)	0.184 (0.012)	0.188 (0.021)	0.144 (0.013)
.15	0.165 (0.007)	0.141 (0.012)	**0.149** (0.030)	0.109 (0.014)
.10	0.112 (0.012)	**0.100** (0.027)	0.084 (0.028)	0.062 (0.015)
.08	**0.092** (0.007)	0.066 (0.017)	0.058 (0.028)	0.043 (0.019)
.06	0.075 (0.010)	**0.060** (0.016)	0.050 (0.033)	0.030 (0.017)
.04	0.056 (0.009)	**0.043** (0.018)	0.025 (0.022)	0.014 (0.019)
.02	**0.018** (0.019)	0.010 (0.013)	0.015 (0.026)	0.007 (0.019)
.01	**0.010** (0.015)	ND	0.007 (0.015)	0.002 (0.016)

the subsimplex spanned by $\{\mathbf{e_1}, \ldots, \mathbf{e_{i-1}}, \mathbf{e_{i+1}}, \ldots, \mathbf{e_p}\}$ have volume V_i. Then

$$a_i^c = \frac{V_i}{\sum_{i=1}^{p} V_i}$$

denotes the abundances of the incenter $\mathbf{c}$. The Euclidean coordinates of the incenter are then given by $\mathbf{c} = \mathbf{E}\mathbf{a^c}$. If a point $\mathbf{x}$ lies in the simplex plane, then the line between $\mathbf{c}$ and $\mathbf{x}$ intersects a certain face of the simplex. The bisective cone of any simplex face is defined as the set of all points for which the connecting line with the incenter intersects that face

$$\mathbf{x} \in Z_i \Leftrightarrow \exists b_1, \ldots, b_p \geq 0 : \begin{cases} \mathbf{x} = \mathbf{c} + \sum_{j=1}^{p} b_j(\mathbf{e_j} - \mathbf{c}) \\ b_i = 0. \end{cases}$$

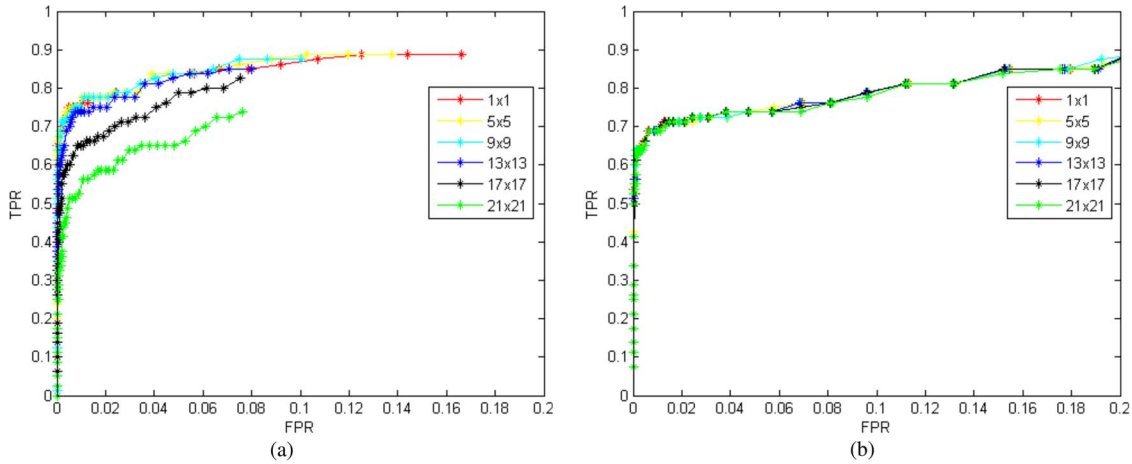

Fig. 4. ROC curves for (a) MF and (b) GMF using different target sizes.

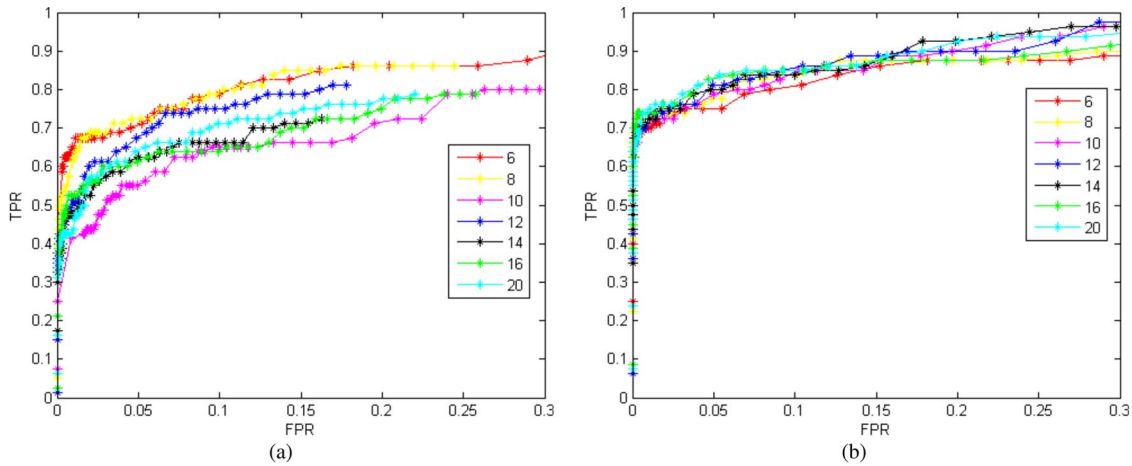

Fig. 5. ROC curves for (a) OSP and (b) GMF using different numbers of endmembers.

In [23], it is shown that, most of the time, a point within the bisective cone Z_i but outside the simplex has an abundance value of zero for endmember $\mathbf{e_i}$. In Fig. 1, this is illustrated.

Since the target is one of the endmembers, the pixels that lie in the bisective cone of the target endmember but outside the simplex belong to the background. Remark that pixels that lie in another bisective cone, and thus have a zero contribution from another endmember, may belong to the background as well, since they may have zero contribution from more than one endmember. These pixels can be found by removing the endmember from which they have zero contribution, and calculate the bisective cones from the reduced (p-2)-dimensional simplex. When the particular pixel then falls in the target bisective cone but outside the simplex, it can be added to the collection of background pixels. If not, the procedure can be repeated. In practice, we found that one iteration delivers sufficient background pixels to proceed.

Using the background pixels identified by the method discussed earlier, the covariance matrix $\tilde{\mathbf{C}}$ of the background is estimated, and the geometric matched filtering score for target endmember $\mathbf{t_s}$ is calculated as

$$\mathrm{GMF}(\mathbf{x}) = \frac{\mathbf{x^T}\tilde{\mathbf{C}}^{-\mathbf{1}}\mathbf{t_s}}{\mathbf{t_s^T}\tilde{\mathbf{C}}^{-\mathbf{1}}\mathbf{t_s}} \gtrless_{H_0}^{H_1} \tau_{\mathrm{GMF}} \tag{5}$$

where, as in MF, the mean spectrum is first subtracted from the data. Since the covariance matrix is estimated from only the pixels that lie in the bisective cone of the target, no target leakage is introduced.

III. Experiments and Results

To demonstrate the performance of the proposed method, hyperspectral data from the Airborne Visible/Infrared Imaging Spectrometer (AVIRIS) cuprite data set, obtained over the Cuprite mining region in Nevada, USA, was used. The data are a 301 $\times$ 365 pixel image with 51 spectral bands in the short-wave infrared range (1.98–2.48 μm). The proposed method is compared to standard matched filtering and OSP. Remark that, in the experiments, any negative outcome of OSP, MF, and geometric MF (GMF) is clipped to zero, which effectively means that the positivity constraint is enforced.

A simulated hyperspectral data cube is generated by implanting a known target spectrum (plastic) in the AVIRIS cuprite data set (as $\gamma \cdot \mathbf{t_s} + (1-\gamma)\cdot$ AVIRIS) with known fractions and at known locations. The mixed pixels are positioned in a total of 80 rectangles of size 21 $\times$ 21 pixels in 8 rows by 10 columns with target fractions varying from 0.20 in the first row to 0.15, 0.10, 0.08, 0.06, 0.04, 0.02, and 0.01 in the following rows. The proposed approach is applied to this data set by combining

the inserted target as an endmember along with a selection of 20 endmembers. This selection was based on an endmember extraction method (vertex component analysis) after which the obtained endmembers were identified by comparison with the U.S. Geological Survey mineral database. To compare, fully constrained least squares unmixing (FCLSU), OSP, and MF are applied as well. To quantify the detection performance of the methods, a ROC curve is generated, in which the true positive rate (TPR) and false positive rate (FPR) are determined for different threshold values (see Fig. 2). In Fig. 3, the obtained detector outputs (where everything below the threshold is clipped to zero) are shown, for a fixed FPR of 0.07. These results show that GMF outperforms the other methods for frequently present target detection.

To validate the performance of the method for partial unmixing, the average and standard deviations of the obtained target fractions (obtained as the output of the filters) from Fig. 3 are given for each row separately in Table I. ND stands for no detection. The total mse values between the obtained and true abundance fractions are 0.0127 for GMF, 0.0135 for FCLSU, 0.0203 for OSP, and 0.0217 for MF.

In a subsequent experiment, we verify that the method still works for "rare" targets. When the size of the rectangles was reduced, the results of GMF converged to those of MF, which can be explained by the fact that, for rare targets, the estimated background agrees more and more with the actual background. In order to show this, we varied the target sizes in the experiment from 1×1 to 21×21 and compared the obtained ROC curves (for GMF, 20 endmembers are applied). In Fig. 4, the obtained ROC curves for MF and GMF are shown.

In order to show that GMF is more robust than OSP against the particular choice of background model, we varied the number of applied endmembers from 5 to 20. In Fig. 5, the obtained ROC curves for OSP and GMF are shown. While the performance of OSP varies severely with different number of endmembers, GMF performs equally well.

IV. Conclusion

In this letter, we have presented a geometric matched filtering technique for targets that are frequently present in the data. The method first projects the data onto the plane of a simplex spanned by background endmembers and target. Then, the background pixels are determined based on the bisective cones of the simplex. Using these background pixels, the MF score for the target endmember is calculated. Experiments on partial unmixing and target detection show that the proposed method outperforms the standard MF and OSP.

References

[1] J. M. Bioucas-Dias *et al.*, "Hyperspectral unmixing overview: Geometrical, statistical, and sparse regression-based approaches," *IEEE J. Sel. Topics Appl. Earth Observ. Remote Sens.*, vol. 5, no. 2, pp. 354–379, Apr. 2012. [Online]. Available: http://oatao.univ-toulouse.fr/5704/1/bioucas_5704.pdf

[2] N. Nasrabadi, "Hyperspectral target detection," *IEEE Signal Process. Mag.*, vol. 31, no. 1, pp. 34–44, Jan. 2014.

[3] J. W. Boardman, F. A. Kruse, and R. O. Green, "Mapping target signatures via partial unmixing of AVIRIS data," in *Proc. Summaries 5th Annu. JPL Airborne Geosci. Workshop*, 1995, vol. 1, pp. 11–14.

[4] J. C. Harsanyi and C. Chang, "Hyperspectral image classification and dimensionality reduction: An orthogonal subspace projection approach," *IEEE Trans. Geosci. Remote Sens.*, vol. 32, no. 4, pp. 779–785, Jul. 1994.

[5] J. Settle, "On the relationship between spectral unmixing and subspace projection," *IEEE Trans. Geosci. Remote Sens.*, vol. 34, no. 4, pp. 1045–1046, Jul. 1996.

[6] D. Manolakis, C. Siracusa, and G. Shaw, "Hyperspectral subpixel target detection using the linear mixing model," *IEEE Trans. Geosci. Remote Sens.*, vol. 39, no. 7, pp. 1392–1409, Jul. 2001.

[7] C. C. Funk, J. Theiler, D. A. Roberts, and C. C. Borel, "Clustering to improve matched filter detection of weak gas plumes in hyperspectral thermal imagery," *IEEE Trans. Geosci. Remote Sens.*, vol. 39, no. 7, pp. 1410–1420, Jul. 2000.

[8] J. Boardman and F. Kruse, "Analysis of imaging spectrometer data using n-dimensional geometry and a mixture-tuned matched filtering approach," *IEEE Trans. Geosci. Remote Sens.*, vol. 49, no. 11, pp. 4138–4152, Nov. 2011.

[9] P. Bajorski, "Analytical comparison of the matched filter and orthogonal subspace projection detectors for hyperspectral images," *IEEE Trans. Geosci. Remote Sens.*, vol. 45, no. 7, pp. 2394–2402, Jul. 2007.

[10] J. B. Broadwater and R. Chellappa, "Hybrid detectors for subpixel targets," *IEEE Trans. Pattern Anal. Mach. Intell.*, vol. 29, no. 11, pp. 1891–1903, Nov. 2007.

[11] A. A. Nielsen, "Spectral mixture analysis: Linear and semi-parametric full and iterated partial unmixing in multi-and hyperspectral image data," *J. Math. Imag. Vis.*, vol. 15, no. 1/2, pp. 17–37, Jul.–Oct. 2001.

[12] J. Settle, "On constrained energy minimization and the partial unmixing of multispectral images," *IEEE Trans. Geosci. Remote Sens.*, vol. 40, no. 3, pp. 718–721, Mar. 2002.

[13] M. D. Farrell and R. M. Mersereau, "On the impact of PCA dimension reduction for hyperspectral detection of difficult targets," *IEEE Geosci. Remote Sens. Lett.*, vol. 2, no. 2, pp. 192–195, Apr. 2005.

[14] Y. Chen, N. Nasrabadi, and T. Tran, "Effects of linear projections on the performance of target detection and classification in hyperspectral imagery," *J. Appl. Remote Sens.*, vol. 5, no. 1, pp. 053563-1–053563-26, Nov. 2011.

[15] P. Bajorski, "Target detection under misspecified models in hyperspectral images," *IEEE J. Sel. Topics Appl. Earth Observ. Remote Sens.*, vol. 5, no. 2, pp. 470–477, Apr. 2012.

[16] Y. Chen, N. Nasrabadi, and T. Tran, "Sparse representation for target detection in hyperspectral imagery," *IEEE J. Sel. Topics Appl. Earth Observ. Remote Sens.*, vol. 5, no. 3, pp. 629–640, Jun. 2011.

[17] Y. S. Matteoli, N. Acito, M. Diana, and G. Corsini, "An automatic approach to adaptive local background estimation and suppression in hyperspectral target detection," *IEEE Trans. Geosci. Remote Sens.*, vol. 49, no. 2, pp. 790–800, Feb. 2011.

[18] R. DiPietro, D. Manolakis, R. Lockwood, T. Cooley, and J. Jacobson, "Hyperspectral matched filter with false-alarm mitigation," *Opt. Eng.*, vol. 51, no. 1, pp. 016202-1–016202-8, Feb. 2012.

[19] P. Schaum and B. J. Daniel, "Continuum fusion methods of spectral detection," *Opt. Eng.*, vol. 51, no. 11, pp. 111718-1–111718-12, Aug. 2012.

[20] Y. Chen, N. M. Nasrabadi, and T. D. Tran, "Kernel sparse representation for hyperspectral target detection," in *Proc. IEEE IGARSS*, 2012, pp. 7484–7487.

[21] Y. Chen, M. N. Nasrabadi, and T. D. Tran, "Simultaneous joint sparsity model for target detection in hyperspectral imagery," *IEEE Trans. Geosci. Remote Sens.*, vol. 8, no. 4, pp. 676–680, Jul. 2011.

[22] D. Manolakis, E. Truslow, M. Pieper, T. Cooley, and M. Brueggeman, "Detection algorithms in hyperspectral imaging systems," *IEEE Signal Process. Mag.*, vol. 31, no. 1, pp. 24–33, Jan. 2014.

[23] R. Heylen, D. Burazerovic, and P. Scheunders, "Fully constrained least-squares spectral unmixing by simplex projection," *IEEE Trans. Geosci. Remote Sens.*, vol. 49, no. 11, pp. 4112–4122, Nov. 2011.